Heterogeneity and anisotropy of the Earth's upper mantle and crust

Andrew Schaeffer[1,2] (aschaeff@cp.dias.ie) and Sergei Lebedev[1]

[(1)]Dublin Institute for Advanced Studies
and [(2)]University College Dublin

SL2013sv: Shear-wave speeds in the Earth's upper mantle

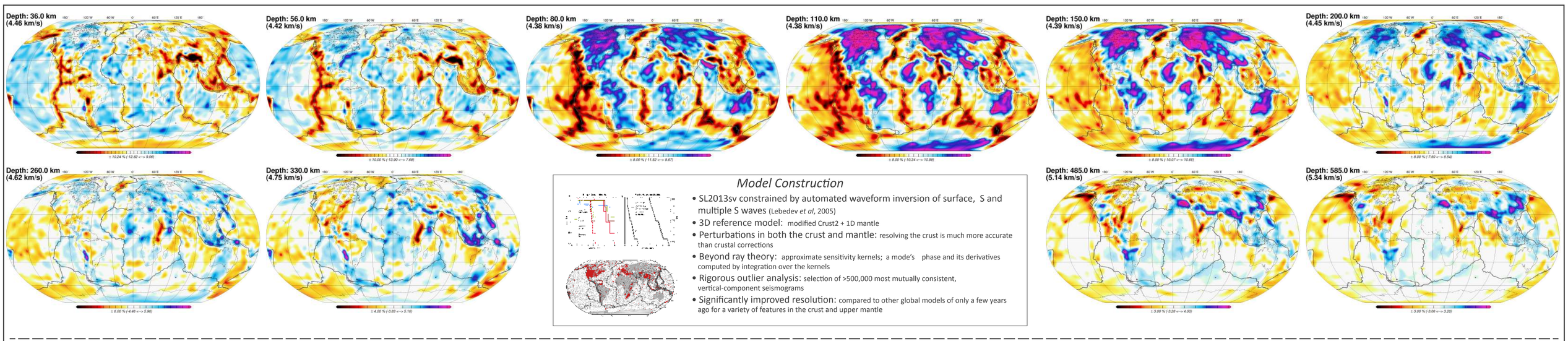

Model Construction

- SL2013sv constrained by automated waveform inversion of surface, S and multiple S waves (Lebedev *et al*, 2005)
- 3D reference model: modified Crust2 + 1D mantle
- Perturbations in both the crust and mantle: resolving the crust is much more accurate than crustal corrections
- Beyond ray theory: approximate sensitivity kernels; a mode's phase and its derivatives computed by integration over the kernels
- Rigorous outlier analysis: selection of >500,000 most mutually consistent, vertical-component seismograms
- Significantly improved resolution: compared to other global models of only a few years ago for a variety of features in the crust and upper mantle

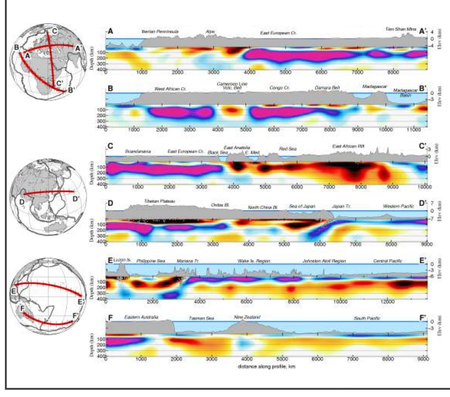

Left: long vertical cross sections through SL2013sv which highlight both fast cratonic roots (A, B, C, D, F), oceanic lithosphere (D, E, F), subduction zones (D, E), and mantle hotspots (C). Close right top: eight cross sections through normal mid ocean ridge segments which demonstrate a triangular shaped low velocity anomaly (red to black) corresponding to the region of partial melting. The strength of the anomalies also show a correlation with spreading rate. Far right: Cross sections through mid ocean ridges which show more complex behaviour, either through interaction with nearby ridge segments or hotspots. Close right bottom: eight cross sections through subduction zones showing clear high-velocity oceanic lithosphere extending through the upper mantle to the transition zone. In all cross sections, seismicity within 40 km laterally is plotted as white circles.

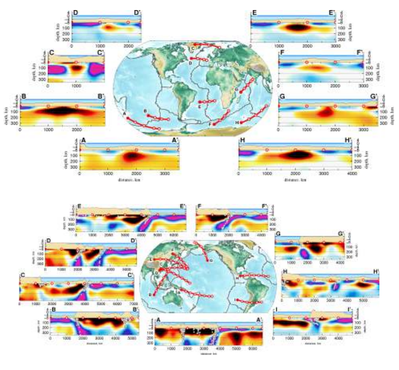

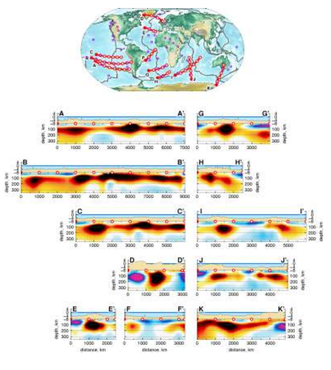

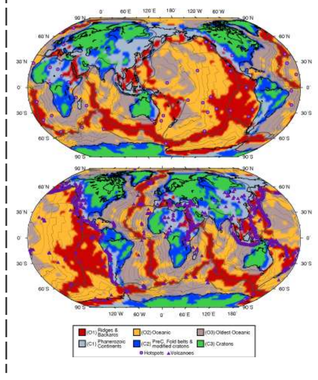

Left: regionalization analysis of SL2013sv (following method of Lekic et al, 2011) into 6 different cluster types. Three oceanic clusters divide the lithosphere based on plate maturity, and three continental clusters divide regions into ancient cratonic, PreCambrian and modified cratonic regions, and Phanerozoic continents. Top-right: 7842 binned 1D shear speed profiles extracted from the triangular spaced model knots of SL2013sv, which demonstrate the bulk distribution of shear velocity as a function of depth in the upper mantle. Bottom-right: shear velocity histograms at ten depths in the upper mantle and transition zone, representing cross sections of the binned profiles above.

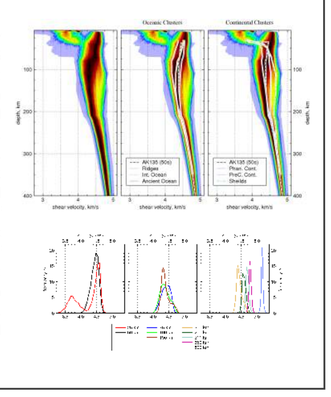

Comparison of Global Models

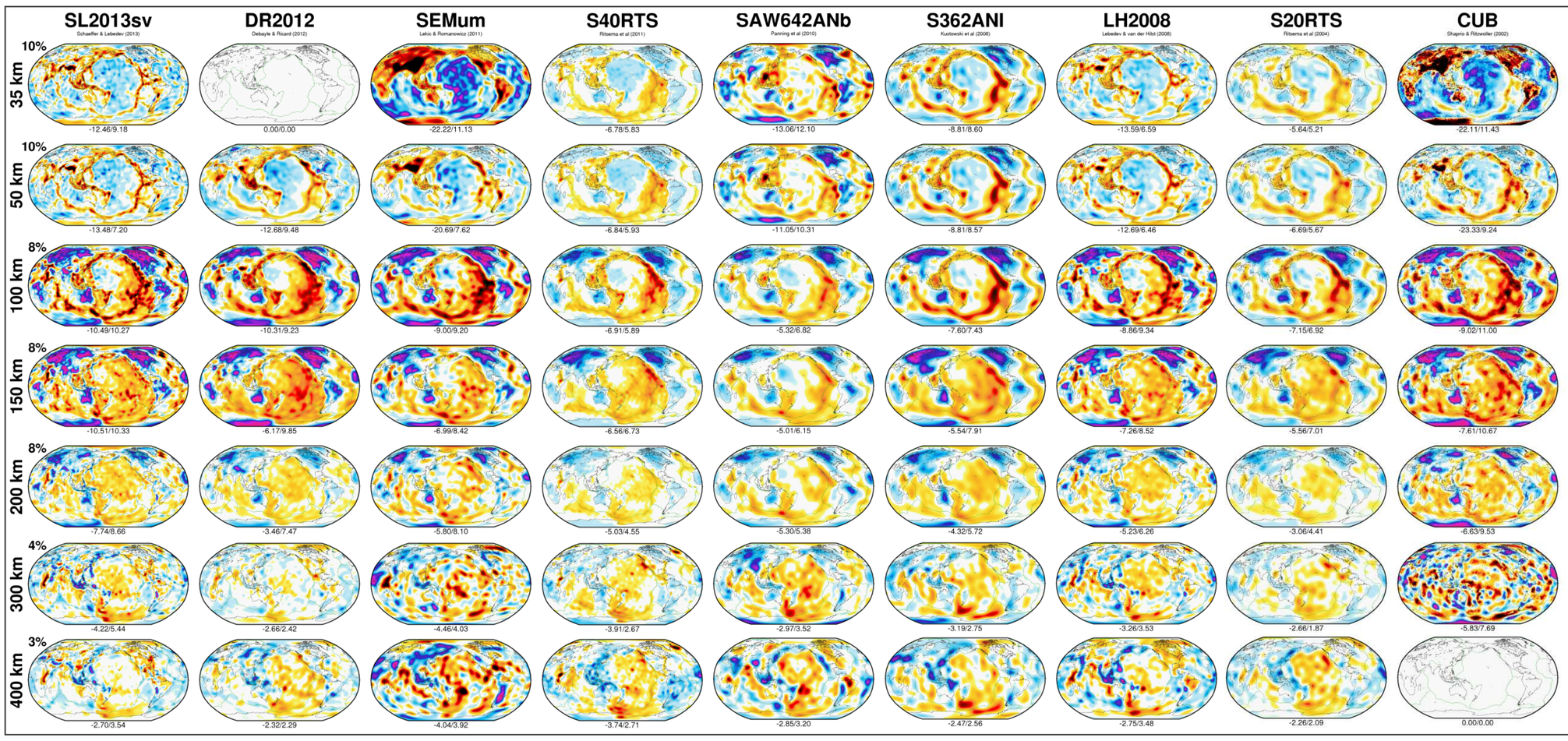

Left: comparison of nine global shear-wave tomography models, plotted at seven depths through the crust and upper mantle. At each depth, perturbations are plotted in per cent with respect to the mean value for that model. Min and max variations are indicated beneath each map. Colour scale saturation is indicated at left for each depth. Long wavelength features are consistent across all models for lithospheric depths (75-200 km), though absolute amplitudes vary substantially. For some models, strong correlations for shorter wavelength features (*ie*, several 100s of km) at 100-150 km depth can be seen (*ex*, SL2013sv, DR2012, SEMum, LH2008, CUB). However, in the deep upper mantle and transition zone (below 250 km depth), large disagreements remain between the different models. Right: RMS velocity perturbation in per cent as a function of depth for the nine models illustrated at left. In most cases, peak RMS values occur at depths between 100 and 150 km. Below: comparison of regionalization of SL2013sv and SEMum with past *a priori* regionalized models GTR1, RUM, and 3SMAC. SL2013sv's and SEMum's regionalizations share a number of common features which differ from the a priori regionalizations, one example being old oceanic lithosphere around the African continent.

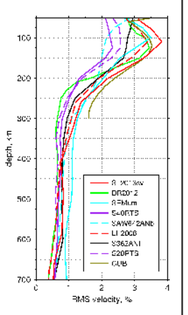

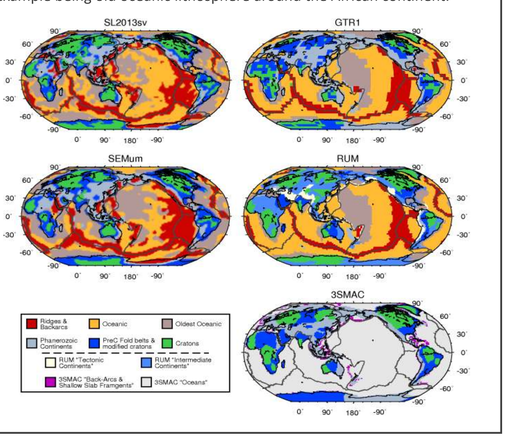

Seismic Anisotropy

Global Anisotropy

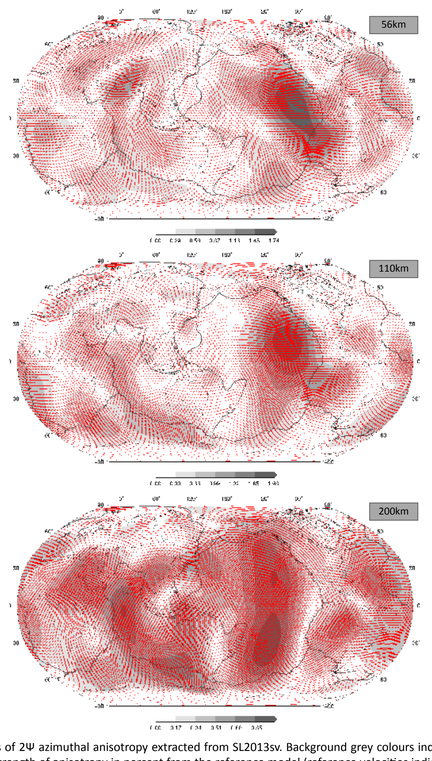

Maps of 2Ψ azimuthal anisotropy extracted from SL2013sv. Background grey colours indicate the strength of anisotropy in percent from the reference model (reference velocities indicated in cross sections at the top). Red sticks show the direction of fast propagation direction, and the length is scaled to the strength of anisotropy. In the inversion, the anisotropy is more strongly smoothed than the isotropic velocity.

Tibet and Eastern Asia

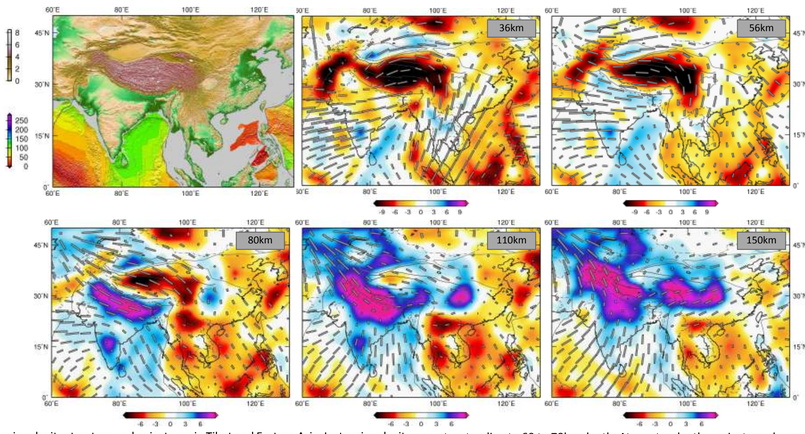

Seismic velocity structure and anisotropy in Tibet and Eastern Asia. Isotropic velocity perturbations extracted from SL2013sv. Azimuthal anisotropy is taken from courser gridded inversino (350 km target spacing), and is represented by grey sticks, with relative size indicating the strength of anisotropy. At shallow depths, rotation of azimuthal anisotropy around the eastern syntaxis of the India-Asia collision is clear, and approximately east-west within the crust of the Tibetan Plateau. A clear bright red low-velocity anomaly beneath the plateau is indicative of the partially molten crust, extending to 60 to 70km depth. At greater depths, anisotropy beneath India rotates to align with its northeastward motion over the last 80 million years, aligning perpendicular to the sea-floor age contours in the map, top left. Several blue-purple high-velocity anomalies are associated with the cold cratonic lithospheres of the Sichuan and Tarim Basins. Also evident is shallow-angle subduction of cold fast Indian lithosphere, extending northwards beneath the Tibetan Plateau.

Western North America

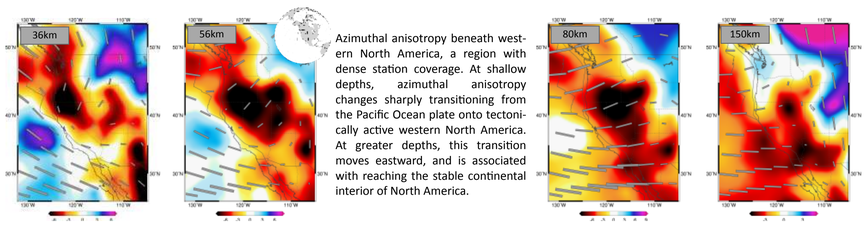

Azimuthal anisotropy beneath western North America, a region with dense station coverage. At shallow depths, azimuthal anisotropy changes sharply transitioning from the Pacific Ocean plate onto tectonically active western North America. At greater depths, this transition moves eastward, and is associated with reaching the stable continental interior of North America.

Pacific Ocean Basin

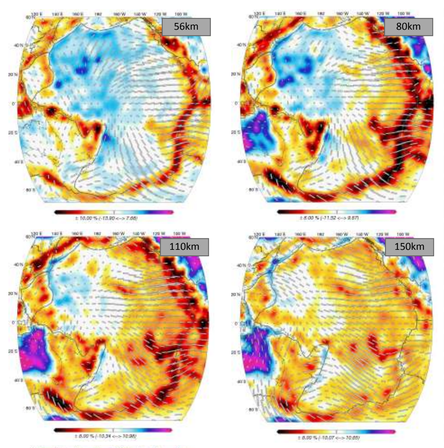

Stratification of azimuthal anisotropy in the Pacific Ocean, as has also been observed in past studies. In the lithosphere, anisotropy is perpendicular to modern spreading ridges in the young eastern Pacific. In the ancient western Pacific, anisotropy follows a different pattern, which correlates with paleo-spreading estimates computed from plate age. In the asthenosphere, anisotropy is parallel with modern day plate motions.

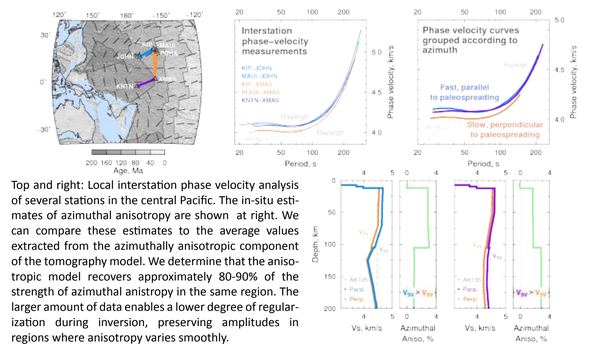

Top and right: Local interstation phase velocity analysis of several stations in the central Pacific. The in-situ estimates of azimuthal anisotropy are shown at right. We can compare these estimates to the average values extracted from the azimuthally anisotropic component of the tomography model. We determine that the anisotropic model recovers approximately 80-90% of the strength of azimuthal anistropy in the same region. The larger amount of data enables a lower degree of regularization during inversion, preserving amplitudes in regions where anisotropy varies smoothly.

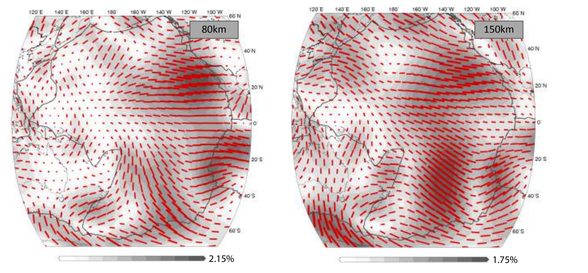

References:

Debayle, E. & Ricard, Y., 2012. A global shear velocity model of the upper mantle from fundamental and higher Rayleigh mode measurements, *J. Geophys. Res.*, **117**.

Gudmundsson, O. & Sambridge, M., 1998. A regionalized upper mantle (RUM) seismic model, *J. Geophys. Res.*, **103**.

Jordan, T. H., 1981. Global tectonic regionalization for seismological data analysis, *B. Seismo. Soc. Am.*, **71 (4)**.

Kustowski, B., Ekstrom, G. & Dziewonski, A.M., 2008. Anisotropic shear-wave velocity structure of the Earth's mantle: a global model, *Geophys. J. Int.*, **174**.

Lebedev, S., Nolet, G., Meier, T. & van der Hilst, R. D., 2005. Automated Multimode Inversion of surface and S waveforms, *Geophys. J. Int.*, **162**.

Lebedev, S. & van der Hilst, R. D., 2008. Global upper-mantle tomography with the automated multimode inversion of surface and S waveforms, *Geophys. J. Int.*, **173**.

Lekic, V. & Romanowicz, B., 2011. Inferring upper-mantle structure by full waveform tomography with the spectral element method, *Geophys J. Int.*, **185**.

Lekic, V. & Romanowicz, B., 2011. Tectonic regionalization without a priori information: A clustering analysis of upper mantle tomography, *Earth Planet Sc. Lett.*, **308**.

Nataf, H. & Ricard, Y., 1996. 3SMAC: an a priori tomographic model of the upper mantle based on geophysical modeling, *Phys. Earth Planet in.*, **9201 (95)**.

Panning, M.P., Lekic, V. & Romanowicz, B., 2010. Importance of crustal corrections in the development of a new global model of radial anisotropy, *J. Geophys. Res.*, **115**.

Ritsema, J., van Heijst, H.J. & Woodhouse, J.H., 2004. Global transition zone tomography, *J. Geophys. Res.*, **109**.

Ritsema, J., Duess, A., van Heijst, H.J. & Woodhouse, J.H., 2011. S40RTS: a degree-40 shear-velocity model for the mantle from new Rayleigh wave dispersion, teleseismic traveltime and normal-mode splitting function measurements, *Geophys. J. Int.*, **108**.

Schaeffer, A. & Lebedev, S., 2013. Global shear speed structure of the upper mantle and transition zone, Geophys. J. Int., In Press

Shapiro, N.M. & Ritzwoller, M.H., 2002. Monte-Carlo inversion for a global shear-velocity model of the crust and upper mantle, *Geophys. J. Int.*, **151**